THE JOURNAL OF PHYSICAL CHEMISTRY B

Article

pubs.acs.org/JPCB

Characteristic Size for Onset of Coffee-Ring Effect in Evaporating Lysozyme-Water Solution Droplets

Heather Meloy Gorr,* Joshua M. Zueger, and John A. Barnard

Department of Mechanical Engineering and Materials Science, University of Pittsburgh, Pittsburgh, Pennsylvania, United States

ABSTRACT: Liquid droplets containing suspended particles deposited on a solid surface often form a ring-like structure due to the redistribution of solute during evaporation, a phenomenon known as the "coffee ring effect". The complex patterns left on the substrate after evaporation are characteristic of the nature of the solute and the particle transport mechanisms. In this study, the morphological evolution and conditions for coffee ring formation for simplified model biological solutions of DI water and lysozyme are examined by AFM and optical microscopy. Lysozyme is a globular protein found in high concentration, for example, in human tears and saliva. The drop diameters studied are very small, ranging from 1 to 50 μm. In this size range, protein motion and the resulting dried residue morphology are highly influenced by the decreased evaporation time of the drop. In this work, we consider the effect of droplet size and concentration on the morphology of the deposited drop as well as the minimal conditions for coffee ring formation in this system. Two distinct deposit types are observed: a simple cap-shaped deposit for drops with small diameters and a ring-like deposit at larger diameters. Ring formation occurs at a critical diameter, which depends systematically on initial lysozyme concentration.

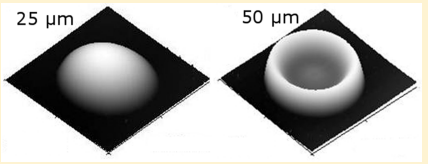

INTRODUCTION

The self-organization of colloidal particles during evaporation of a sessile droplet leads to interesting patterns in the resulting deposit. When the contact line is pinned during evaporation, solute particles generally accumulate in a ring around the periphery of the drop due to the "coffee ring" effect. Deegan et al.[1−3] first explained this ring-like deposit, which is attributed to capillary flows induced by nonuniform evaporation of the pinned droplet. This phenomenon is relevant to a variety of technologies, including ink jet printing[4,5] and DNA microarray printing.[6] In addition, there has been recent interest in studying the solute patterns from evaporation of biological fluids. The unique patterns that form in biofluids may act as markers for various pathological processes. This has recently been demonstrated in drops of blood serum,[7,8] synovial fluids,[9] tears,[10,11] and whole blood.[12,13] Thus, understanding and quantifying these patterns, via image analysis or pattern recognition techniques, for example,[8,14] may be valuable in diagnostic applications.

Recent studies on the physical mechanisms of sessile droplet evaporation[15−20] demonstrate that the resulting patterns are influenced by multiple factors, including capillary flow,[15−17] Marangoni flow,[18] advection−diffusion of particles,[19,21] particle−substrate interactions,[22,23] and particle−particle interactions.[24] Phase transition phenomena have also been reported during evaporation of colloidal sessile droplets as a result of the increase in solute concentration during evaporation. For example, gel or glassy transitions have been observed in polymer solutions[25−27] and in drops of whole blood.[13,14] In these solutions, a gel-like "skin" forms at the periphery of the drop while the "coffee ring" develops and the gelation front moves inward as evaporation proceeds. Formation of a "skin" was also observed in drops of ellipsoidal particle suspensions,[24] where a loosely packed structure formed at the air−water interface and resisted ring formation.

Although ring formation has been demonstrated in a variety of systems, a uniform film is often preferred in applications such as printing and coatings. Techniques have been developed to control the patterns in the deposit by manipulating the evaporative flux,[3,28] particle−substrate interactions,[22,23] and the physiochemical properties of the solution.[4,24,29,30] Uniform deposits have been observed in colloidal silica[4] and polymer suspensions,[28,30] where the final pattern depends on the composition of the solution. Final shapes of the deposits have also been predicted numerically.[23,27] Bhardwaj et al.[23] proposed that the uniform deposit resulted when attractive DLVO interactions between the particles and substrate dominate over radial outward flow and Marangoni convection. The deposit shape was recently predicted in polymer solutions based on the ratio of the initial and gelation concentrations.[27] Higher ratios of initial to gelation concentration resulted in more uniform, dome-like deposits, while lower ratios resulted in ring-shaped deposits due to suppression of the radial flow near the gelation concentration.

Understanding pattern formation in micro- and nanoscale systems is relevant to a variety of phenomena such as nanoparticle self-assembly, micro-, and nanofluidics. However, the literature is dominated by the study of macroscopic droplets (on the order of millimeters). Several studies have examined patterns in microscale drops,[5,21,22,31−33] but a physical interpretation of the dynamics in these smaller scale drops is not yet fully established. Prior work in our group[34−36] focused on drops with diameters less than 50 μm, using dilute solutions

Received: August 9, 2012
Revised: September 20, 2012
Published: September 21, 2012

dx.doi.org/10.1021/jp307933a | J. Phys. Chem. B 2012, 116, 12213−12220

of dendrimer molecules in alcohol. It was demonstrated that pattern formation in this system depended sensitively on the evaporation time. This was also established recently by Shen et al.,[21] who studied microscale drops of solutions of colloidal PS spheres. Although these well-studied systems tend to produce ring-shaped deposits, the deposits from very small drops (with diameters less than ~10 μm) did not exhibit the typical ring-like shape. A minimum droplet diameter was found to exist for ring formation at the microscale. For drops with diameters less than this critical value, the particles were dispersed homogenously on the substrate. This type of deposit was formed when the liquid evaporated faster than the rate of particle diffusive motion.[21]

In this study, the effects of droplet size and concentration on the final shapes of deposits resulting from evaporation of dilute aqueous solutions of lysozyme are explored. Lysozyme is a protein found in high concentration in human biological fluids such as tears[12,37,38] and saliva.[39] In recent investigations,[40] we found that the overall lysozyme residue morphology was ring-like with an undulating interior, which varied little with concentration. However, the final packing of lysozyme molecules was strongly dependent on initial concentration which was attributed to the formation of a gel during evaporation. Here, the deposit shape is examined using Atomic Force Microscopy (AFM) for small drop diameters ranging from 1 to 50 μm. A transition from a simple cap-shaped deposit to a ring-like deposit occurs at a critical diameter, which depends systematically on initial lysozyme concentration.

EXPERIMENTAL SECTION

Lysozyme. Lysozyme is a globular protein found in high concentration in human mucosal secretions, such as tears[12,37,38] and saliva.[39] It is the most abundant protein in tears, with a concentration of ~2 mg/mL.[12] This well-studied protein has a roughly ellipsoidal shape with approximate dimensions of 3.0 × 3.0 × 4.5 nm, molecular mass of 14 kDa, and carries a net positive charge at physiological pH.[41] Lysozyme has been the subject of many protein crystallization[42−45] and self-assembly[46−49] studies. The gelation of lysozyme[43,50] can be brought about by changes in temperature, pH, and ionic strength, and by the addition of a solvent resulting in a transparent, viscoelastic, gel matrix.[51] Lysozyme molecules have been known to adsorb to various substrates as monomers and no large-scale conformational changes have been reported from solution to adsorption.

Solutions. Lysozyme solutions were prepared using high purity lysozyme powder obtained from Sigma Aldrich (catalog no. L6876) with no further purification. A single batch of lysozyme powder was used in all of the solutions reported here. As-received powder was dissolved in deionized water (Millipore, resistivity of 18.2 MΩ·cm) at 35 °C to concentrations (ρ) 0.1, 0.25, 0.5, 0.75, and 1.0 g/100 mL and stored at 2 °C. Solutions were brought to room temperature prior to deposition. Note that commercial lysozyme powder contains salts for purification and buffering purposes.[52,53] The concentration of salts in commercial lysozyme has been previously measured using X-ray fluorescence and was found to range from 3.6% to 10.2% (w/w) of chloride, or up to 46 mols of chloride per 1 mol of lysozyme.[53]

Substrates and Deposition Techniques. Silicon wafer substrates were cleaned ultrasonically (Fisher Scientific, FS20) in iso-propyl alcohol (IPA), then acetone, and finally rinsed with DI water and blown dry using compressed air. Small drops were deposited onto the clean wafers using two different methods to produce a wide range of drop diameters: an aerosol spray system (Preval) and a nebulizer (Omron, NE-U22 V), both obtained from AnalTech, Inc. The aerosol system produced droplets yielding dried residue diameters from ~10 to 250 μm in diameter and the droplets produced by the nebulizer ranged from ~1 to 30 μm. Drops evaporated from the substrate under ambient conditions. Deposition patterns were stable for at least 8 weeks, verified by periodic optical and atomic force microscopy measurements during this time period.

Characterization. A drop shape analysis (DSA) system (Kruss, D100) was used to determine the wetting properties and surface tension of aqueous lysozyme solutions on clean Si wafer substrates. By the sessile drop method, the contact angle, θ, drop diameter, D, and drop volume, V_D, for macroscopic drops are measured as a function of time. The initial contact angle of sessile drops of lysozyme solutions on silicon wafers was ~55°; little dependence on solution concentration was found.

The dried deposits from small drops were characterized in air by AFM (Digital Instruments, D3100) in tapping mode with a standard tip (K-TEK Nanotechnology, LLC, NSG01). At least 20 drops of each concentration were characterized. The raw AFM data were analyzed using Gwyddion SPM software. First, obvious scanning defects such as artifacts and scan lines were removed. A small neighborhood of pixels containing the erroneous data was selected and a hyperbolic flatten function was used to interpolate the pixel information from the surrounding area. The data were then leveled using a plane level function which computes the plane from all of the data points and subtracts the plane from the original data. This corrects for slight drift but does not suppress the features or texture of the surface.[54] Finally, the minimum pixel value was set as the plane of the substrate (z = 0).

Although the resolution of the AFM is on the order of fractions of a nanometer, uncertainties in these measurements should be noted. The local measurement uncertainty can be estimated from instrument calibration data, following the method described in Klapetek et al.[55] This method was implemented in Gwyddion; the measurement uncertainty is added to AFM measurement results and propagated through the statistical functions as the data is processed.

RESULTS

Deposit Shapes. Deposits from evaporated lysozyme solution droplets with diameter, D, ranging from 1 to 50 μm were studied by AFM for concentrations ρ = 0.1, 0.25, 0.5, 0.75, and 1.0 g/100 mL. Two characteristic deposit morphologies are noted: a simple, cap-shaped deposit in very small drops and a ring-like deposit as D increases. The generally observed cap and ring deposits for ρ = 1.0 g/100 mL are illustrated in Figure 1 using two- and three-dimensional AFM topographic images and cross-sectional profile plots.

The cap and ring forms illustrated in Figure 1 were consistently observed throughout this study. Note that the z-axis scales in Figure 1 are in nanometers, whereas the dimensions in the plane of the substrate are in micrometers. Both deposits are radially symmetric and cover the entire wetted area. The deposit in Figure 1a has the shape of a spherical cap with a maximum height of ~225 nm and shows no indication of ring formation. We refer to this shape as the "cap-like" shape throughout this paper. The typical "ring-like" deposit is illustrated in Figure 1b. A single, well-defined "coffee

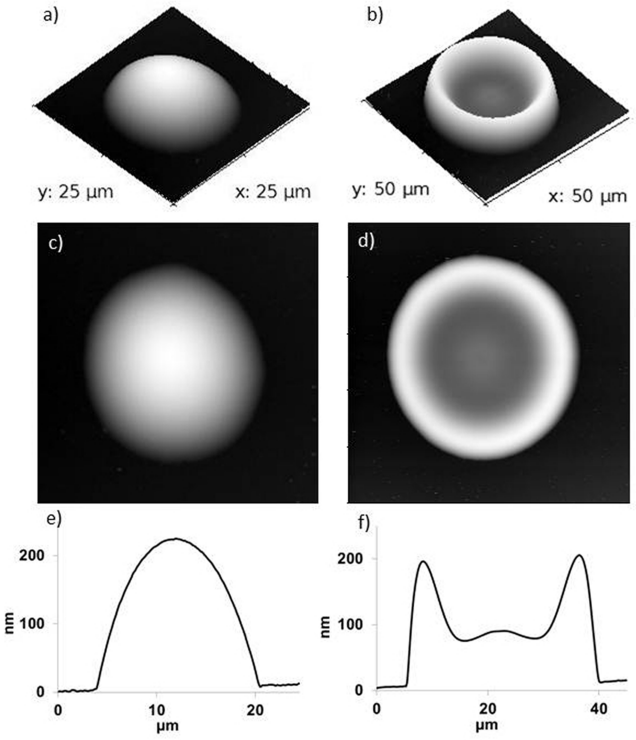

Figure 1. Representative morphologies for uniform and ring shaped deposits with ρ = 1.0 g/100 mL. Parts (a), (c), and (e) illustrate a typical cap-shaped deposit with D = 17.2 μm and parts (b), (d), and (f) correspond to a typical ring-shaped deposit with D = 35.8 μm. Top row: 3-D view of AFM topography, middle row: plan-view AFM topography, bottom row: AFM cross-section.

ring" is present at the perimeter of the deposit. From the maximum height at the peak of the ring (here about 200 nm), the profile drops to a minimum and then rises slightly in the central region (Figure 1f).

Critical Diameter for Ring Formation. After surveying the shapes of a large number of drops of different sizes, it became clear that a transition from cap-like to ring-like deposits occurred at a well-defined D. This transition is illustrated in Figure 2 for drops with diameters ranging from ~1 to 20 μm for solution concentration ρ = 0.5 g/100 mL.

For this concentration, the 1 and 5 μm deposits (Figure 2a,b) are below the minimum size for ring formation. At $D \approx 10$ μm (Figure 2c), a very small, circular depression is visible in the central region of the deposit. The existence of a local minimum in the AFM cross section (not shown here) indicates the onset of ring formation in this system and is referred to as the critical diameter for ring formation, D_c. As D increases, the ring becomes more pronounced. For example, the 15 μm deposit (Figure 2d) is ring-like with a circular depression in the center. The 20 μm deposit (Figure 2e) has a well-defined ring-like shape with the typical undulation in the central region. This shape is consistent with the profiles found for all drops with D > 20 μm at this concentration. Although the transition between the cap and ring-like shapes is gradual, the deposit is referred to as "ring-like" if a local minimum exists near the center of the deposit.

Effect of Concentration. The transition between the two shape regimes was clearly observed in all concentrations studied. However, the critical diameter for ring formation systematically increased with initial lysozyme concentration. To illustrate this phenomenon, representative drops from concentrations ρ = 0.1, 0.5, and 1.0 g/100 mL are collected in Figure 3 for $D \approx$ 5, 10, 15, 20, and 25 μm.

The deposits are cap-like for all three concentrations for D < 5 μm. The coffee ring shape begins to form at a critical diameter, D_C, which depends on initial solution concentration and is indicated by the dotted line in Figure 3. As the concentration increases, D_C increases. The drops with $D \approx 25$ μm have very similar topography, independent of concentration. To examine these shapes more closely, AFM cross sectional profiles are presented in Figure 4.

The profiles of the smallest drops in Figure 4a ($D \approx 5$ μm) have cap-like shapes for ρ = 0.5 and 1.0 g/100 mL, but the shape has a local minimum in the center for the lowest concentration (ρ = 0.1 g/100 mL), indicating the development of a ring. This is considered the critical diameter, D_C for the ρ = 0.1 g/100 mL concentration. In Figure 4b, the 0.5 g/100 mL deposit has a local minimum in the center, indicating ring formation. The 0.1 g/100 mL deposit has a well-defined ring shape while the highest concentration deposit (1.0 g/100 mL) has a cap-like shape at this diameter. In Figure 4c, the highest concentration deposit has a local minimum, indicating ring formation. The two deposits with lower concentrations exhibit the well-defined ring-like shape with the central mound. Despite the difference in concentration, these two deposits are quite similar in shape. This is illustrated further in Figure 4d, which contains the cross-sectional profiles for drops with $D \approx 30$ μm. All three concentrations have deposits with similar ring-like shapes. These patterns show negligible concentration dependence in the geometry of the deposit for drops with D > 25 μm for all concentrations in this study. This observation is consistent with the findings in our previous study for drops with $30 \leq D \leq 50$ μm.[40]

DISCUSSION

Ring Formation. Formation of the ring-like deposit is discussed in our previous work[40] and is briefly summarized here. When the droplet is deposited, lysozyme molecules adsorb to the Si wafer substrate, pinning the droplet. The liquid

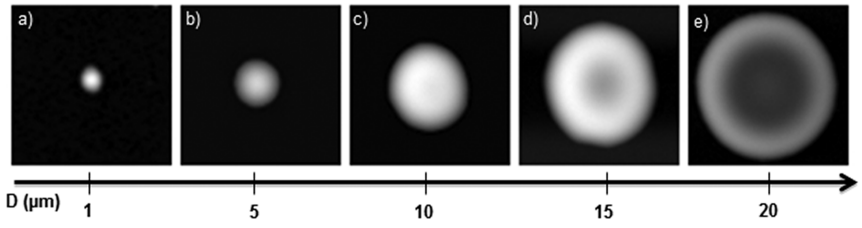

Figure 2. AFM topographic images of lysozyme droplet deposits (ρ = 0.5 g/100 mL) with increasing diameter. Approximate diameters are indicated in μm.

dx.doi.org/10.1021/jp307933a | J. Phys. Chem. B 2012, 116, 12213−12220

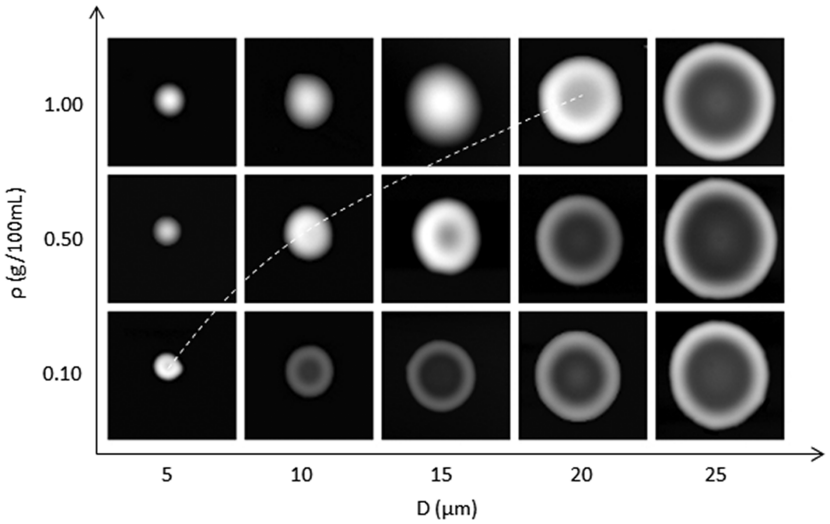

Figure 3. AFM topographic maps for droplets in rows with increasing ρ and in columns from left to right with increasing $D \approx 5$, 10, 15, 20, and 25 μm. The dotted line approximates the critical diameter for coffee ring formation, D_C.

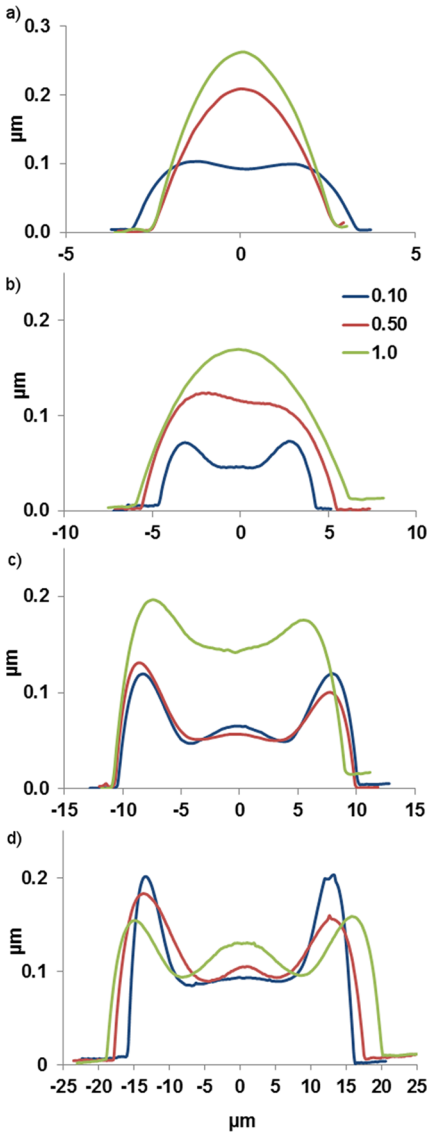

Figure 4. AFM cross sectional profiles for deposits with $D \approx 5$, 10, 20, and 30 μm for solution concentrations ρ = 0.1, 0.5, 1.0 g/100 mL.

drop maintains a spherical cap shape and the contact angle decreases during evaporation. Radial flows carry unadsorbed molecules to the perimeter of the drop where the flux is the highest, consistent with the "coffee ring effect." Simultaneously, lysozyme molecules collect at the air–water interface,[56,57] forming a loosely packed, permeable skin. Lysozyme molecules accumulate at the periphery, undergoing a gel transition which proceeds inward toward the center of the drop. The contact angle continues to decrease until a critical angle, θ_r, is reached. At this point, the remaining liquid depins and recedes toward the center of the drop. The residual lysozyme in this liquid collects in the mound shape on top of the gel structure, forming the well-defined ring-like shape.

In our previous study, it was noted that the ring-like deposit geometry is quite similar for all concentrations, but the volume fraction of lysozyme molecules in the deposit increased linearly with initial solution concentration. This was attributed to the formation of the gel phase throughout the deposit. Thus, drops with higher initial lysozyme solution concentrations produce a denser, much more tightly packed deposit, though the overall morphology is similar to those of the lower concentration solutions. Similar ring heights and widths were observed across the range of concentrations, determined by the geometry of the liquid droplet during evaporation and the angle at which the depinning event occurs, θ_r.

Evaporation of drops with $D < 50$ μm is difficult to observe in situ. Therefore, mm-scale drops of the same lysozyme/DI water solutions were used to visualize the morphological evolution during evaporation by drop shape analysis (DSA). Several time sequence images illustrating the shape evolution are shown in Figure 5.

The contact angle decreases linearly with time (Figure 5a–d) while evaporation proceeds. Gel formation in the perimeter ring is apparent in Figure 5e. The remaining liquid depins (Figure 5e) and recedes (Figure 5f–i) more rapidly. The final ring-like deposit is shown in Figure 5i. The overall shape of the final deposit in Figure 5 is consistent with the ring-like deposits for $D < 50$ μm and thus the evaporation process is assumed to be similar in the two size ranges. Although no direct measurements were made on drops with $D < 50$ μm, the initial contact angle is assumed to be ~55°, as measured by DSA. However, some natural variation from droplet to droplet

dx.doi.org/10.1021/jp307933a | J. Phys. Chem. B 2012, 116, 12213–12220

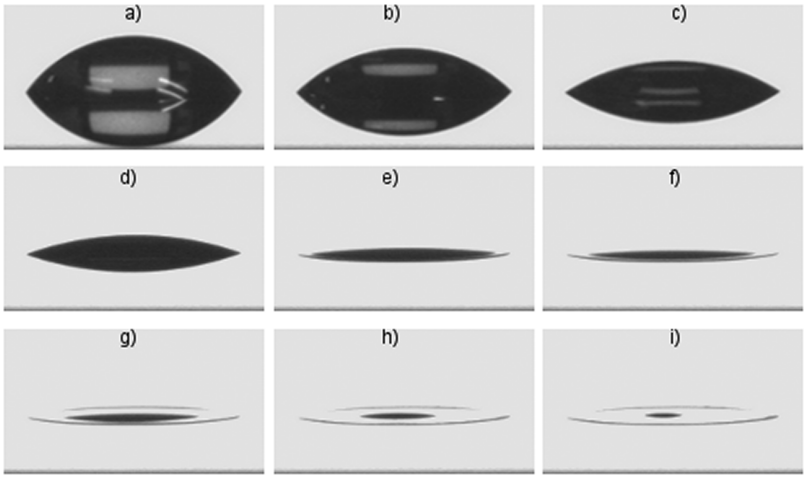

Figure 5. Shape evolution of lysozyme/DI water solution droplet (ρ = 1.0 g/100 mL, $D \approx 3$ mm) at times of (a) ~0.5, (b) 5, (c) 10, (d) 15, (e) 20, (f) 21, (g) 22, (h) 23, and (i) 24 min.

is expected due to local substrate heterogeneities and the nature of the deposition process in this experiment.

Particle Transport. The deposits in this study are clearly influenced by the characteristic time and length scales of the experiment. We assume that macroscopic models of evaporation are applicable in this case, as the mean free path of the vapor molecules is significantly less than the length scale in our experiments and therefore within the regime of continuum mechanics. The droplet evaporation time scale can be estimated using the evaporation model proposed by Popov:[16]

$$\tau = \frac{\pi \rho_L R^2 \theta_0}{16 D_V (c_o - c_\infty)}$$

where D_V is the diffusion coefficient of the vapor in air, c_o is the density of saturated vapor immediately above the liquid–air interface, c_∞ is the ambient vapor density, ρ_L is the liquid density, θ_0 is the initial contact angle, and R the drop radius. On the basis of the parameters of our experiment, the time scale for evaporation is on the order of seconds. The velocity of the radial flow can be estimated by $u \approx j/\rho_L$, where j is the solvent evaporation rate:[17]

$$j(r) = \frac{2}{\pi} \frac{D_V (c_0 - c_\infty)}{(R^2 - r^2)^{1/2}}$$

In our case, $u \approx 8$ μm/s near the center of the drop, which is consistent with particle velocities observed in evaporating biofluid drops.[13]

To determine the time and length scales for lysozyme diffusion, we find the mean displacement of lysozyme monomers during evaporation, X_L. This is estimated using the Stokes–Einstein equation and the expected diffusion coefficient for lysozyme monomers in solution,[58] $D_L \approx 1 \times 10^{-10}$ m^2/s:

$$X_L = (6 D_L \tau)^{(1/2)}$$

The mean displacement due to diffusion can be compared to two other length scales, the mean spacing of molecules in solution and the size of the drop. Assuming a homogeneous distribution of lysozyme particles in solution, the mean distance between two lysozyme monomers in the liquid suspension, λ_L, is estimated by the following:

$$\lambda_L = \left(\frac{V_d}{n_L} \right)^{(3/2)}$$

where V_d is the volume of the liquid drop and n_L is the number of lysozyme molecules in the liquid drop per unit volume. V_d is determined using an initial contact angle of ~55° and assuming the contact diameter is equal to the deposit diameter. The number of lysozyme molecules per unit volume, n_L, is estimated from the initial solute concentration. Considering the lysozyme concentrations in our experiments, $\lambda_L \approx 10$–30 nm and based on the estimated evaporation time for a drop with $D = 50$ μm, we find a maximum of $X_L \approx 15$ μm. Thus, this system can be considered "crowded" for the solution concentrations and drop diameters studied, as the average spacing of lysozyme molecules in solution is much less than mean-squared displacement of particles over the time scale of the experiment.[58] In other words, to travel the characteristic length, every lysozyme molecule will travel many times the nearest neighbor distance and potentially interact with many other lysozyme molecules. During evaporation, the effective concentration of lysozyme within the drop increases and the diffusion coefficient will decrease due to self-obstruction in the crowded system. As the diffusion coefficient approaches zero, the system approaches kinetic arrest and the sol–gel transition takes place at a critical volume fraction or gelation concentration, φ_g.

Shape Transition. Uniform, dome-like[4,23,28,30] and pillar-like deposits[59,60] have been observed in a number of systems and were predicted based on consideration of the dominant transport mechanisms in the droplet. For example, uniform deposits occur when Marangoni convection dominates over radial flow[4,28,30] and when DLVO interactions between the particles and substrate dominate over the radial outward flow and Marangoni convection.[23] The deposit shape has also been predicted numerically based on the ratio of the initial and gelation concentrations in polymer solutions.[27] A dome-like shape resulted when the radial flow was suppressed due to gelation in drops with higher initial polymer concentrations.

The deposit shape has recently been discussed by comparing the representative time scales for evaporation and diffusion.[21,60] This reasoning is employed here in describing the lysozyme deposit shapes. The shapes can be analyzed in terms of the competition between advection and diffusion of the lysozyme molecules. In the pinned droplet, unadsorbed lysozyme

molecules will be influenced by radial capillary flow, which is opposed by particle diffusion. For the ring to form, the "coffee ring effect" must be greater than the effect of diffusion. A more homogeneous deposit would be expected when diffusion dominates over capillary flow.

The competition between advection and diffusion can be examined using the dimensionless Peclet number. Following the solutions and scaling of the Navier–Stokes equations:[61]

$$\mathrm{Pe} = \frac{uL}{D_L}$$

where u is the particle velocity, L is the characteristic size of the system, and D_L is the particle diffusion coefficient. In general, when Pe $\gg$ 1 advection dominates transport and when Pe $\ll$ 1, diffusion is the dominant mechanism. To find the Peclet number in our system, we estimate the radial velocity as u = 8 μm/s. The radius of the drop is taken as the characteristic length of the system, L, and we assume the reported diffusion coefficient of lysozyme monomers as $D_L = 1 \times 10^{-10}$ m^2/s.[58] On the basis of these assumptions, the Peclet number for the range of diameters in this experiment is Pe = 0.05 − 2.00. The range of Peclet numbers at this scale indicates that both advection and diffusion are occurring in competition. Pe was determined for all deposits examined in this experiment and is plotted in Figure 6 as a function of initial concentration. The deposits with a ring-like shape are indicated with a circle and the cap-like shapes are indicated with a triangle.

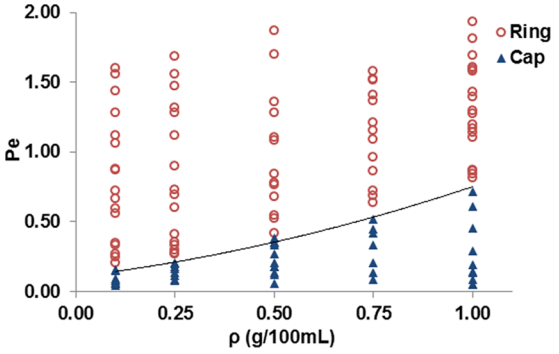

Figure 6. Plot of Peclet numbers for concentrations ρ = 0.1, 0.25, 0.5, 0.75, and 1.0 g/100 mL. Open circles represent ring-like deposits while the solid triangles represent cap-like deposits. The fit line indicates the transition between the two deposit types.

Several trends can be seen in Figure 6, which shows the transition between the deposit shapes for each concentration, as indicated by the fit line. The deposits with Pe < 0.20 for all concentrations have cap-like shapes, while all of the deposits with Pe > 1 are ring-like. Between Pe $\approx$ 0.20 − 0.80, the transition occurs at different values depending on the concentration.

In this system, a Peclet number of 1 corresponds to a characteristic length of 12.5 μm, or D = 25 μm. This is generally consistent with our experimental observations, as the deposits with D > 20 μm (corresponding to Pe > 1) have ring-like shapes. In other words, when the Peclet number is greater than 1 in this system, advection is dominant, which drives ring formation. As Pe $\rightarrow$ 0, diffusion becomes more dominant, which is also consistent with our observations. The absence of the coffee ring in very small drops (with low Pe) indicates that diffusion is the dominant transport mechanism in this case.

Deposit Contact Angle. In ring-like deposits, the lysozyme collects at the periphery and begins to gel. When the contact angle reaches the critical angle, θ_r, the liquid depins and recedes, leaving deposits with similar volume and geometry, independent of initial concentration (higher initial lysozyme concentrations yield more densely packed final deposits). For the cap-like shapes, the behavior is different. Although the general shape is similar for all cap-like deposits, the AFM measured contact angle of the *deposit* (and therefore the volume of the cap) increases with solution concentration. We propose that when $D < D_c$ (cap-like deposits), the gelation concentration throughout the deposit, φ_g, is reached before the receding contact angle, θ_r, is reached, and that the time to reach φ_g decreases with concentration. To examine this hypothesis further, the contact angle of the deposit, θ_D, was determined by fitting the AFM cross sectional profiles to a spherical cap shape, taking θ_D as the maximum angle with the horizontal. These values are plotted in Figure 7 as a function of D for the deposit shapes observed in this study.

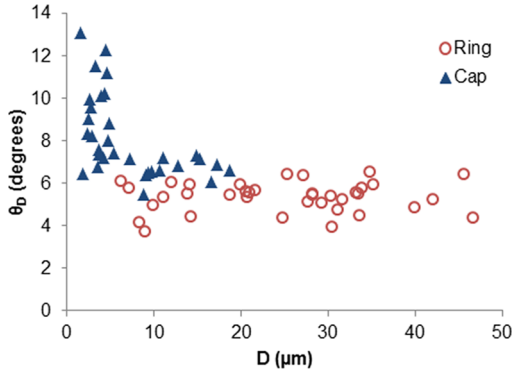

Figure 7. Contact angle of the deposit, θ_D, vs diameter, D, for all concentrations studied. Open circles represent ring-like deposits while the solid triangles represent cap-like deposits.

In ring-like deposits, θ_D varied within a narrow band from approximately 3°–6° for all concentrations. The contact angles of the cap-shaped deposits are larger, ranging from ~6° to 15°, depending on diameter and initial solution concentration. In cap-like deposits, the angle increased with increasing concentration. On the basis of these observations, we assume that the critical receding contact angle, $\theta_r \approx 6°$. The scatter in the data likely reflects typical experimental error such as local substrate heterogeneities and slight variations in concentration and evaporation rate from droplet to droplet due to the nature of the deposition process.

In general, cap-like deposits are formed when the gel transition occurs before the drop shape reaches θ_r. In the case of the evaporating droplet, the diffusion coefficient is dependent on concentration and time. Due to crowding and DLVO interactions, the lysozyme diffusion coefficient decreases with increasing concentration.[58,62] In drops with higher protein concentrations, there is a higher degree of self-association and the system will reach kinetic arrest before the more dilute concentrations. Therefore, drops with higher concentrations will undergo the gel transition at an earlier time in the evaporation process. The diameter for ring formation is thus larger in solutions with higher lysozyme concentrations.

dx.doi.org/10.1021/jp307933a | J. Phys. Chem. B 2012, 116, 12213–12220

CONCLUSIONS

In this work, the formation of cap-like and ring-like deposits of microscale aqueous lysozyme droplets has been documented. In this system, a critical diameter, D_c, exists for ring formation, which depends on initial lysozyme concentration. The initial aqueous lysozyme sessile droplet shape is a spherical cap with a contact angle of ~55°, which decreases during evaporation. Lysozyme adsorbs to the Si substrate, pinning the droplet, and also collects at the air−water interface, forming a permeable skin. The remaining lysozyme is free to diffuse or be influenced by radial flows.

When $D > D_c$, ring-like shapes are formed due to the transport of molecules to the periphery by capillary flow. The drop undergoes a phase transition, beginning from the highly concentrated ring area and moving inward toward the center of the still-liquid drop. When the contact angle reaches a critical value, the remaining liquid depins and recedes toward the center of the droplet. The geometry of the lysozyme deposit is ring-like with an undulating interior and does not dependent on concentration. This was found for drops with $D > 20$ μm.

When $D < D_c$, the deposit is uniform with a cap-like shape. This shape occurs when diffusion is the dominant transport mechanism in this system. The transition between the two regimes can be described by finding the Peclet number for the experimental system. When Pe > 1, the deposit is ring-like as a result of radial flow. When Pe < 1, the deposit patterns are strongly dependent on concentration, with diffusion playing a major role in the transport of lysozyme particles. As Pe decreases, the deposit shapes become cap-like as a result of the dominant diffusive transport. As the initial lysozyme concentration increases, the critical diameter for ring formation also increases. In this paper, we propose that the concentration dependent cap-like deposit is due to the droplet reaching the gelation concentration before the contact angle reaches the critical receding angle, θ_r.

AUTHOR INFORMATION

Corresponding Author

*E-mail: hlm32@pitt.edu.

Notes

The authors declare no competing financial interest.

ACKNOWLEDGMENTS

The authors acknowledge the facilities and scientific and technical assistance of the Materials Micro-Characterization Laboratory of the Department of Mechanical Engineering and Materials Science, Swanson School of Engineering, University of Pittsburgh.

REFERENCES

(1) Deegan, R. D.; Bakajin, O.; Dupont, T. F.; Huber, G.; Nagel, S. R.; Witten, T. A. *Nature* **1997**, *389*, 827−829.
(2) Deegan, R. D. *Phys. Rev. E* **2000**, *61* (1), 475−485.
(3) Deegan, R. D.; Bakajin, O.; Dupont, T. F.; Huber, G.; Nagel, S. R.; Witten, T. A. *Phys. Rev. E* **2000**, *62* (1), 756−762.
(4) Park, J.; Moon, J. *Langmuir* **2006**, *22*, 3506−3513.
(5) Zhou, J. X.; Fuh, J. Y. H.; Loh, H. T.; Wong, Y. S.; Ng, Y. S.; Gray, J. J.; Chua, S. J. *Int. J. Adv. Manuf. Technol.* **2010**, *48*, 243−250.
(6) Dugas, V.; Broutin, J.; Souteyrand, E. *Langmuir* **2005**, *21*, 9130−9136.
(7) Yakhno, T. A.; Yakhno, V. G.; Sanin, A. G.; Sanina, O. A.; Pelyushenko, A. S.; Egorova, N. A.; Terentiev, I. G.; Smetanina, S. V.; Korochkina, O. V.; Yashukova, E. V. *IEEE Eng. Med. Biol.* **2005**, *24* (2), 96−104.
(8) Killeen, A. A.; Ossina, N.; McGlennen, R. C.; Minnerath, S.; Borgos, J.; Alexandrov, V.; Sarvazyan, A. *Mol. Diagn. Ther.* **2006**, *10* (6), 371−380.
(9) Esmonde-White, K. A.; Mandair, G. S.; Raaii, F.; Jacobson, J. A.; Miller, B. S.; Urquhart, A. G.; Roessler, B. J.; Morris, M. D. *J. Biomed. Opt.* **2009**, *14* (3), 034013.
(10) Shabalin, V. N.; Shatokhina, S. N. *Singapore Med. J.* **2007**, *48* (5), 440−446.
(11) Kuo, M.-T.; Lin, C.-C.; Liu, H.-Y.; Chang, H.-C. *Invest. Ophth. Vis. Sci.* **2011**, *52* (7), 4942−4950.
(12) Brutin, D.; Sobac, B.; Loquet, B.; Sampol, J. *J. Fluid Mech.* **2011**, *667*, 85−95.
(13) Sobac, B.; Brutin, D. *Phys. Rev. E* **2011**, *84*, 011603.
(14) Kim, N.; Zhenguo, L.; Hurth, C.; Zenhausern, F.; Chang, S.; Attinger, D. *Anal. Methods* **2012**, *4*, 50−57.
(15) Fischer, B. J. *Langmuir* **2002**, *18*, 60−67.
(16) Popov, Y. O. *Phys. Rev. E* **2005**, *71*, 36313.
(17) Hu, H.; Larson, R. G. *Langmuir* **2005**, *21*, 3963−3971.
(18) Hu, H.; Larson, R. G. *J. Phys. Chem. B* **2006**, *110*, 7090−7094.
(19) Bhardwaj, R.; Fang, X.; Attinger, D. *New J. Phys.* **2009**, *11*, 075020−075053.
(20) Girard, F.; Antoni, M. *Langmuir* **2008**, *24*, 11342−11345.
(21) Shen, X.; Ho, C.-M.; Wong, T.-S. *J. Phys. Chem. B* **2010**, *114*, 5269−5274.
(22) Andreeva, L. V.; Koshkin, A. V.; Lebedev-Stepanov, P. V.; Petrov, A. N.; Alfimov, M. V. *Colloids Surf. A* **2007**, *300*, 300−306.
(23) Bhardwaj, R.; Fang, X.; Somasundaran, P.; Attinger, D. *Langmuir* **2010**, *26* (11), 7833−7842.
(24) Yunker, P. J.; Still, T.; Lohr, M. A.; Yodh, A. G. *Nature* **2011**, *476*, 308−311.
(25) Pauchard, L.; Allain, C. *Phys. Rev. E* **2003**, *68*, 052801.
(26) Gorand, Y.; Pauchard, L.; Calligari, G.; Hulin, J. P.; Allain, C. *Langmuir* **2004**, *20*, 5138−5140.
(27) Okuzono, T.; Kobayashi, M.; Doi, M. *Phys. Rev. E* **2009**, *80*, 021603.
(28) Kajiya, T.; Kobayashi, W.; Okuzono, T.; Doi, M. *Langmuir* **2010**, *26* (13), 10429−10432.
(29) Yan, Q.; Gao, L.; Sharma, V.; Chiang, Y.-M.; Wong, C. C. *Langmuir* **2008**, *24*, 11518−11522.
(30) Kajiya, T.; Kobayashi, W.; Okuzono, T.; Doi, M. *J. Phys. Chem. B* **2009**, *113*, 15460−15466.
(31) Socol, Y.; Guzman, I. S. *J. Phys. Chem. B* **2006**, *110*, 18347−18350.
(32) Sangani, A. S.; Lu, C.; Su, K.; Schwarz, J. A. *Phys. Rev. E* **2009**, *80*, 011603.
(33) Wong, T.-S.; Chen, T.-H.; Shen, X.; Ho, C.-M. *Anal. Chem.* **2011**, *83* (6), 1871−1873.
(34) Li, F.-I.; Thaler, S. M.; Leo, P. H.; Barnard, J. A. *J. Phys. Chem. B* **2006**, *110* (51), 25838−25843.
(35) Li, F.-I.; Leo, P. H.; Barnard, J. A. *J. Phys. Chem. C* **2008**, *112* (37), 14266−14273.
(36) Li, F.-I.; Leo, P. H.; Barnard, J. A. *J Phys Chem B* **2008**, *112* (51), 16497−16504.
(37) Ronen, D.; Eylan, E.; Romano, A.; Stein, R.; Modan, M. *Invest. Ophth.* **1975**, *14* (6), 479−484.
(38) Fullard, R. J.; Snyder, C. *Invest. Ophth. Vis. Sci* **1990**, *31* (6), 1119−1126.
(39) Yeh, C.-K.; Dodds, M. W. J.; Zuo, P.; Johnson, D. A. *Arch. Oral. Biol.* **1997**, *42* (1), 25−31.
(40) Gorr, H. M.; Zueger, J. M.; Barnard, J. A. *Langmuir* **2012**, *28* (9), 4039−4042.
(41) Blake, C. C. F.; Koenig, D. F.; Mair, G. A.; North, A. C. T.; Phillips, D. C.; Sarma, V. R. *Nature* **1965**, *206*, 757−761.
(42) Pusey, M. L.; Snyder, R. S.; Naumann, R. *J. Biol. Chem.* **1986**, *261* (14), 6524−6529.
(43) Muschol, M.; Rosenberger, F. *J. Chem. Phys.* **1997**, *107* (6), 1953−1962.

(44) Georgalis, Y.; Umbach, P.; Soumpasis, D. M.; Saenger, W. *J. Am. Chem. Soc.* **1998**, *120*, 5539−5548.
(45) Heijna, M. C. R.; Theelen, M. J.; van Enckevort, W. J. P.; Vlieg, E. *J. Phys. Chem. B* **2007**, *111*, 1567−1573.
(46) Stradner, A.; Sedgwick, H.; Cardinaux, F.; Poon, W. C. K.; Egelhaaf, S. U.; Schurtenberger, P. *Nature* **2004**, *432*, 492−495.
(47) Cardinaux, F.; Stradner, A.; Schurtenberger, P.; Sciortino, F.; Zaccarelli, E. *Europhys. Lett.* **2007**, *77*, 48004.
(48) Rozhkov, S. P.; Goryunov, A. S. *Biophys. Chem.* **2010**, *151*, 22−28.
(49) Cardinaux, F.; Zaccarelli, E.; Stradner, A.; Bucciarelli, S.; Farago, B.; Egelhaaf, S.; Sciortino, F.; Schurtenberger, P. *J. Phys. Chem. B.* **2011**, *115*, 7227−7237.
(50) Yan, H.; Saiani, A.; Gough, J. E.; Miller, A. F. *Biomacromolecules* **2006**, *7*, 2776−2782.
(51) da Silva, M. A.; Areas, E. P. G. *J. Colloid Interface Sci.* **2005**, *289*, 394−401.
(52) Retailleau, P.; Ries-Kautt, M.; Ducruix, A. *Biophys. J.* **1997**, *73*, 2156−2163.
(53) Jolivalt, C.; Ries-Kautt, M.; Chevallier, P.; Ducruix, A. *J. Synchrotron Rad.* **1997**, *4*, 28−35.
(54) Klapetek, P.; Necas, D.; Anderson, C. *Data Leveling and Background Subtraction*. http://gwyddion.net/documentation/user-guide-en/.
(55) Klapetek, P.; Nečas, D.; Campbellová, A.; Yacoot, A.; Koenders, L. *Meas. Sci. Technol.* **2011**, *22*, 48004.
(56) Sundaram, S.; Ferri, J. K.; Vollhardt, D.; Stebe, K. J. *Langmuir* **1998**, *14*, 1208−1218.
(57) Alahverdjieva, V. S.; Grigoriev, D. O.; Ferri, J. K.; Fainerman, V. B.; Aksenenko, E. V.; Leser, M. E.; Michel, M.; Miller, R. *Colloids Surf. A* **2008**, *323*, 167−174.
(58) Price, W. S.; Tsuchiya, F.; Arata, Y. *J. Am. Chem. Soc.* **1999**, *121* (49), 11503−11512.
(59) Willmer, D. I.; Baldwin, K. A.; Kwartnik, C.; Fairhurst, D. J. *Phys. Chem. Chem. Phys.* **2010**, *12*, 3998−4004.
(60) Baldwin, K. A.; Granjard, M.; Willmer, D. I.; Sefiane, K.; Fairhurst, D. J. *Soft Matter* **2011**, *7*, 7819−7826.
(61) Maki, K. L.; Kumar, S. *Langmuir* **2011**, *27*, 11347−11363.
(62) Nesmelova, I. V.; Skirda, V. D.; Fedotov, V. D. *Biopolymers* **2002**, *63*, 132−140.